# Electronic structure of the misfit-layer compounds $PbTiS_3$ and $SnNbS_3$

Youichi Ohno
*Department of Physics, Faculty of General Education, Utsunomiya University, 350 Mine-machi, Utsunomiya, Tochigi 321, Japan*
(Received 26 November 1990)

The compounds $PbTiS_3$ and $SnNbS_3$ may be classified as misfit-layer compounds with compositions $(PbS)_{1+x}TiS_2$ or $(SnS)_{1+x}NbS_2$. Their structure is such that a double layer of PbS or SnS with the TlI structure is inserted into each van der Waals gap of a layered transition-metal disulfide. They may be regarded as intercalation compounds or as materials having a one-dimensional superlattice with an atomic-scale repeat distance. X-ray-photoemission-spectroscopy, x-ray-absorption-spectroscopy, and reflection-electron-energy-loss-spectroscopy spectra are presented and the electronic structures are discussed. It is found that charge transfer occurs from the PbS or SnS layers to the transition-metal disulfide slabs, but the interlayer interaction is so small that the overall features of the valence and conduction bands of each layer are considered to be almost unchanged from those of the bulk compound.

## I. INTRODUCTION

$PbTiS_3$ and its family of related compounds crystallize in the orthorhombic or the slightly-distorted monoclinic structure isotypic with $LaCrS_3$, wherein the LaS and $CrS_2$ layers are alternately stacked. They are misfit-layer compounds with nonstoichiometric compositions, denoted by $(MS)_{1+x}(TS_2)$. The structure of $TiS_2$ layer is the same as that of a slab within layered group-IVa transition-metal disulfides in which cationic atoms are surrounded octahedrally by six sulfur atoms. The atomic arrangement within each PbS layer is the same as that in a double layer in TlI, which is approximately obtained by slicing a rocksaltlike lattice with two planes perpendicular to a $\langle 001 \rangle$ direction and having the interplanar distance of half a lattice constant. The crystal structure of $PbTiS_3$ is shown in Fig. 1. $SnNbS_3$ is isomorphic with $PbTiS_3$, but within a $NbS_2$ layer Nb atoms are trigonal-prismatically coordinated to six S atoms. The crystal structure of $SnNbS_3$ is shown in Fig. 2.

Since 1966 when the compounds were synthesized by Sterzel,[1] several works on the crystal growth[2–4] and electrical properties[5–7] have been done. However, a precise determination of the crystal structure had not been made until an x-ray analysis was carried out for the single crystals of $SnNbS_3$ and $LaNbS_3$ by Wiegers and co-workers[8–10] and by Meerschaut and co-workers[11,12] in 1988. Preliminary electrical measurements have been done by Schmidt and co-workers[5,6] for the powder samples of this group. They behaved as superconductors at low temperature, for example, $SnNbS_3$ exhibited superconducting property at 2.75 K which was slightly lower than the critical temperature of $NbS_2$ while $PbTaS_3$ had the temperature of 3.07 K which was higher than that of $TaS_2$. Normal conductivity parallel to the layers is larger by about $10^5$ than the perpendicular one, reflecting the electrical property of each of the alternating layers. $NbS_2$ or $TaS_2$ layers with metallic conductance govern high conductivity parallel to the layers and SnS or PbS layers with semiconducting high electrical resistance governs low conductivity perpendicular to the layers. For $SnNbS_3$ the Seebeck coefficient and the magnetic susceptibility have been measured by Wiegers *et al.*[8] Their be-

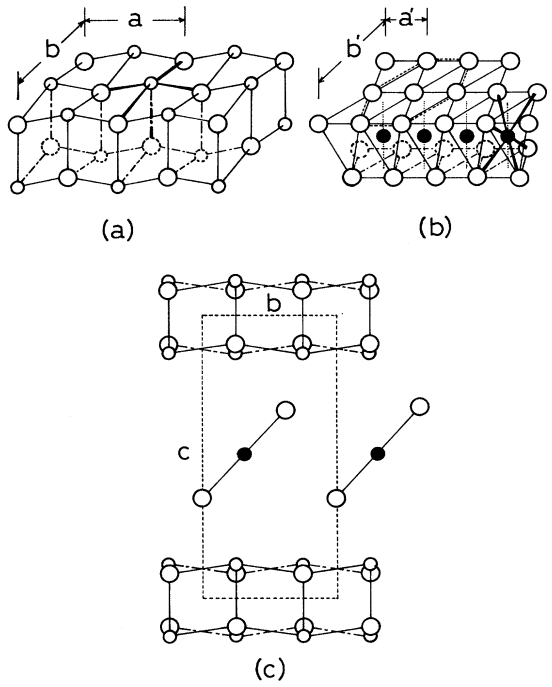


FIG. 1. Crystal structure of $PbTiS_3$. (a) PbS layer which is the same atomic arrangement as a double layer in TlI. (b) $TiS_2$ layer, in which Ti atoms are surrounded octahedrally by six S atoms. (c) (100) section. A dotted line denotes the unit cell of $PbTiS_3$. Both the lattices of PbS and $TiS_2$ layers have *C*-centered orthorhombic unit cells which match along the *b* and *c* axes but not along the *a* axis.

 

havior is quite similar to that of the intercalation compounds of $NbS_2$. These facts suggest that interlayer interaction is so small that we may consider each of the layers to be very weakly bonded electronically to its adjacent layers. However, it may be expected that charge transfer occurs from one layer to another by the difference in chemical potentials or the Fermi levels. Thus the compounds may be regarded as intercalation compounds of layered transition-metal disulfides. The SnS or PbS molecules are, in this case, considered to be intercalates forming an ordered double layer within van der Waals gaps. From a different point of view, they can be regarded as materials having a one-dimensional superlattice with an atomic-scale repeat distance. In this case each layer would possess a more perfect atomic arrangement and crystal habit as compared with artificial superlattices prepared by means of the molecular beam epitaxy method, the metalorganic chemical vapor deposition method, and so on, because they are grown as single crystals under near-equilibrium conditions. As far as the present author knows, the energy band structures as well as the optical properties have not been studied.

This paper presents x-ray-photoemission-spectroscopy (XPS), x-ray-absorption-spectroscopy (XAS), and reflection-electron-energy-loss spectroscopy (REELS) studies of $PbTiS_3$ and $SnNbS_3$ and discusses the electronic structure, drawing upon knowledge of existing band calculations and experimental results of the bulk compounds of each layer or related compounds with similar band structures. In Sec. II we describe the growth of the single crystals, sample preparations for the experiments, and apparatus used here. We also describe procedures for determining the binding energies of core electrons and optical densities. In Sec. III experimental results obtained here are discussed. In Sec. III A $PbTiS_3$ will be discussed and in Sec. III B $SnNbS_3$ will be discussed.

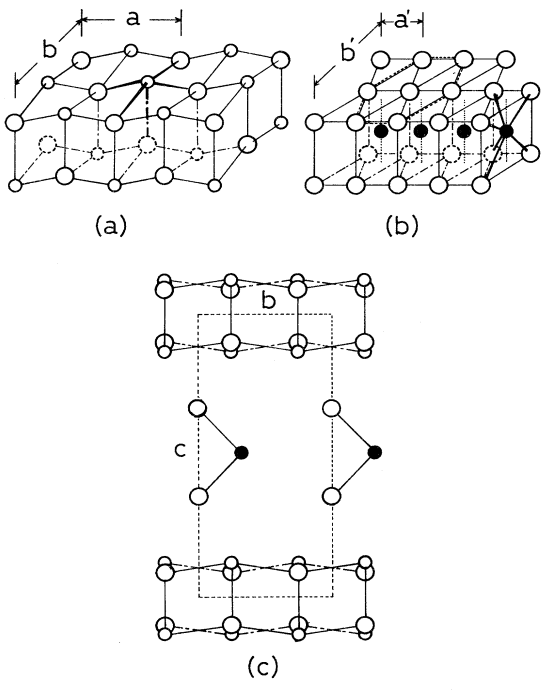


FIG. 2. Crystal structure of $SnNbS_3$. (a) SnS layer, which has the same atomic arrangement as a double layer in $\beta$-SnS. (b) $NbS_2$ layer, in which Nb atoms are trigonal-prismatically coordinated to six S atoms. (c) (100) section. A dotted line denotes the unit cell of $SnNbS_3$. Both the lattices of SnS and $NbS_2$ have $C$-centered orthorhombic unit cells which match along the $b$ and $c$ axes but not along the $a$ axis.

## II. EXPERIMENTS

The single crystals of $PbTiS_3$ and $SnNbS_3$ were grown by a chemical vapor transport reaction in an evacuated and then closed silica ampoule with inner-diameter of 15 mm and length of about 300 mm. The mixing ratios of constituent elements were determined, assuming the following reactions:

$$TiS_2 + x\,PbS + y\,PbCl_2 + y\,S \rightarrow PbTiS_3 + y\,Cl_2 \quad (1)$$

and

$$Nb + x\,Sn + y\,SnBr_2 + y\,S \rightarrow SnNbS_3 + y\,Br_2\ , \quad (2)$$

where $x+y=1$ and $y=0.08-0.18$ and $Cl_2$ and $Br_2$ on the right-hand side were employed as a transport agent. The elements on the left-hand side were placed in a high-temperature zone of a three-zone electric furnace. In the first step they were heated for a week at 730 °C for $PbTiS_3$ and at 850 °C for $SnNbS_3$. A final temperature gradient for crystal growth was 800–700 °C for $PbTiS_3$ and 840–770 °C for $SnNbS_3$. After a month large single crystals were grown in both temperature zones; in the low-temperature zone the crystals were grown in a straight or curved ribbonlike form, the maximum length being about 20 mm, while in the high-temperature zone they were grown in a layer form, the diameter being about 10 mm.

The structural determination and the chemical analysis were done by means of the x-ray powder-diffraction and the XPS techniques. Our powder-diffraction pattern of $PbTiS_3$ was quite similar to that of Sterzel and Horn.[2] A detailed comparison of our diffraction data for $SnNbS_3$ with those of Wiegers and co-workers[8–10] could not be made because the (001) diffraction peaks corresponding to cleaved surfaces appeared very intense relative to the other peaks. However, all diffraction peaks observed were well indexed, using their lattice constants. Figure 3 shows the XPS spectra of $PbTiS_3$ and $SnNbS_3$ in a long-range scanning. They are compared with the XPS spectrum of $PbZrS_3$ which crystallizes in the $NH_4CdCl_3$ structure and has a simple chemical composition (atomic ratio 1:1:3). Such a comparison gives a rough estimate for the chemical compositions of $PbTiS_3$ and $SnNbS_3$. We believe that the compounds have a chemical composition as expected from the formula. Atomically clean and smooth surfaces for XPS and REELS measurements were prepared by cleaving with adhesive tape in the atmosphere just before the measurements. Auger electron spectroscopy (AES) spectra as well as the core-electron

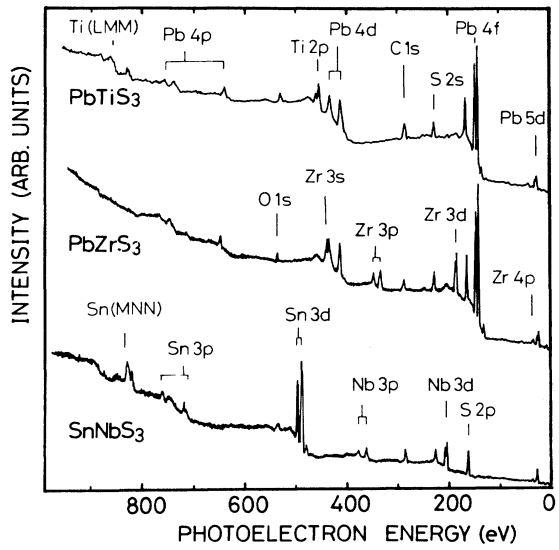


FIG. 3. Core-electron XPS spectra in a long-range scanning of $PbTiS_3$ and $SnNbS_3$. They are compared with the XPS spectrum of $PbZrS_3$ which crystallizes in the $NH_4CdCl_3$ structure with the chemical composition of the integer ratio 1:1:3. No corrections have been made for photoemission cross sections, but the comparison gives a rough estimate for the chemical compositions of $PbTiS_3$ and $SnNbS_3$.

XPS spectra displayed small carbon and oxygen contaminant peaks, but the argon-ion sputtering and subsequent annealing technique, which was customarily used for surface cleaning, was not used, because it caused a surface disorder and a nonstoichiometric surface chemical composition.

The binding energies of the core electrons and the densities of states of the valence bands were measured by photoemission with unmonochromatized Mg $K\alpha$ radiation (excitation energy of 1253.6 eV). An x-ray generator used here was commercially available and equipped with both Al and Mg anodes. Its operation was made under the conditions of 15 kV and 20 mA. Ejected and reflected electrons from a surface were energy analyzed with a double-pass cylindrical mirror analyzer (CMA) (Perkin Elmer Instruments, model 15-255G). The binding energies of deep core electrons were measured with respect to the Fermi level of a spectrometer, using C 1$s$ (284.6 eV) and Ag $3d_{5/2}$ (368.2 eV) lines as a reference line, while the binding energies of shallower Sn 4$d$ and Pb 5$d$ electrons were measured with respect to the top of the valence band. A vacuum system and a data acquisition and processing system are in common with the REELS ones which have been described in other papers.[13,14]

Core and valence electrons' excitation REELS spectra were measured with a normal-incidence electron gun coaxial to the CMA. To obtain the second-derivative spectra, the measurements were carried out in the voltage modulation mode with use of a lock-in amplifier. A modulation voltage was 1 V peak to peak. Energy resolution increases with decreasing incident energy $E_0$.

The partial densities of states of conduction bands were measured by means of the XAS method. A vacuum soft-x-ray absorption spectrometer used here was of the Johann type with a Rowland circle with 30 cm radius. Anode and filament materials were tungsten and a dispersing crystal was quartz with a $(10\bar{1}1)$ face. The operating conditions of an x-ray tube were 4.0 kV and 25 mA and a base pressure in operation was less than $3\times10^{-4}$ Pa. Photon signals passing through a preamplifier and a pulse-height analyzer were accumulated by a scalar during the preset time of 30 s and then input to a personal computer (NEC PC9801 RA2) via a RC-232C interface. Photon energy was step scanned by a pulse motor combined with a goniometer. The final spectra were obtained by accumulating ten data sets for each spectrum. They were drawn on an $X$-$Y$ plotter as normalized optical density versus photon energy. Here the normalized optical density is given by

$$J(E)=\frac{\ln[I_0(E)/I(E)]-\ln[I_0(E_n)/I(E_n)]}{\ln[I_0(E_m)/I(E_m)]-\ln[I_0(E_n)/I(E_n)]}\ , \qquad (3)$$

where $I_0(E)$ and $I(E)$ are the intensities of incident and transmitted x-ray beams and $E_m$ and $E_n$ are the energies at which maximum and minimum absorption occurs, respectively. Energy resolution in a S $K$ region was about 1.2 eV.

## III. RESULTS AND DISCUSSION

### A. $PbTiS_3$

As described above the crystal of $PbTiS_3$ is constructed of alternately stacked PbS and $TiS_2$ layers. We have firstly investigated interlayer interaction and bonding between constituent atoms within each layer by the core-electron XPS method. Table I tabulates the binding energies of the core electrons, which have been compared with those of PbS and $TiS_2$ and the x-ray-absorption edges of $TiS_2$. The binding energies for PbS have been obtained by Shalvoy, Fisher, and Stiles[15] with respect to the Fermi level of a spectrometer, using the Ag $3d_{5/2}$ line as a reference line. The binding energies for $TiS_2$ have been obtained by Endo *et al.*,[16] who have, however, given no descriptions on the origin of its energy scale. Within the sudden approximation the x-ray-absorption edges[17,18] give the energy difference between the ground state of an excited electron and the Fermi level of a material because $TiS_2$ exhibits metallic properties. Although there are some problems in direct comparisons, we find a good agreement among them, especially, for electrons with large binding energies. In a small binding-energy region far from the reference line, we observe systematic errors of about 0.5 eV. They are not caused by chemical shifts because the disagreement occurs for both cationic and anionic atoms to a similar extent. If we take the errors into account, we may suggest that bonding within the layers remains almost unchanged from that of the bulk compounds. The S 2$p$ XPS spectrum reveals only the two peaks related to spin-orbit components, but does

TABLE I. Binding energies in eV of core electrons of $PbTiS_3$, PbS, and $TiS_2$ and x-ray-absorption edges of $TiS_2$.

| Core electron | $PbTiS_3$ | PbS[a] | | $TiS_2$ |
|---|---|---|---|---|
| Pb $4f_{7/2}$ | 137.0 | 137.6 | | |
| Pb $4f_{5/2}$ | 141.9 | 142.4 | | |
| S $2p_{3/2}$ | 160.2 | 160.8 | 161.1[b] | 159.6–160.7 ($L_3$ edge)[c,d] |
| S $2p_{1/2}$ | 161.4 | | 162.1 | 161.8 ($L_2$ edge)[d] |
| S $2s$ | 224.7 | 225.1 | | |
| Pb $4d_{5/2}$ | 412.4 | 412.6 | | |
| Pb $4d_{3/2}$ | 434.7 | | | |
| Ti $2p_{3/2}$ | 455.9 | | 456.0 | 455.9 ($L_3$ edge)[c] |
| Ti $2p_{1/2}$ | 461.9 | | 462.3 | |

[a]Shalvoy, Fisher, and Stiles, Ref. 15.
[b]Endo *et al.*, Ref. 16.
[c]Fischer, Ref. 17
[d]Sonntag and Brown, Ref. 18.

not show the additional peaks arising from different chemical circumstances. This fact implies that electron population of S atoms within a PbS layer is similar to that within a $TiS_2$ layer, which is supported from the agreement between the binding energies of the bulk compounds (see Table I). The core-electron XPS results give no evidences for interlayer interaction. We may conclude that bonding between the layers is much weaker than ionic-covalent bonding within the layers. This conclusion may be supported by the fact that the crystal is easily cleaved parallel to the layers.

Figure 4 shows the valence-band XPS spectrum of $PbTiS_3$, compared with those of $TiS_2$ and PbS which have, respectively, been measured by Wertheim, DiSalvo, and Buchanan[19] and McFeely *et al.*[20] with monochromatized x-ray beams. The origin of the horizontal axis is the photoemission thresholds of $PbTiS_3$ and PbS. Since the spectrum of $TiS_2$ has been drawn, aligning its main peak with the corresponding large peak of $PbTiS_3$, the Fermi level is located at 0.7 eV below the origin. As a result we may propose that charge transfer occurs from PbS to $TiS_2$ layers by different chemical potentials. The main features of the XPS spectra are summarized in Table II. Since the energy band structures of PbS and $TiS_2$ have been extensively studied theoretically and experimentally,[22–26] then the comparison makes it possible to assign the main features without difficulties. The peak at the 10.3 eV is attributed to a Mg $K\alpha_{3,4}$ satellite due to excitation of Pb $5d$ core electrons with unmonochromatized x-ray beams. The Pb $5d_{5/2}$ and $5d_{3/2}$ electrons exist at 18.6 and 21.2 eV below the top of the valence band, respectively, and the Mg $K\alpha_{3,4}$ satellite peaks appear around 8.4 and 10.2 eV below the main peak. The other structures are assigned, based on the energy band structure of each layer. The results are summarized in the last column in Table II. Here, the Pb $3s$ peak of PbS layers is found to be shifted by 0.6 eV on the smaller binding-energy side. This shift may be artificial due to overlapping the Mg $K\alpha_{3,4}$ satellite. The overall valence-band structure is well represented by simple superposition of energy bands of each layer. We may suggest that the top of the valence band consists of the Ti $3d$ $t_{2g}$ band of $TiS_2$ layers and the S $3p$ bonding band of PbS layers.

Figure 5 shows the S $K$ XAS spectrum in $PbTiS_3$, which has been compared with those in PbS, $TiS_2$, and

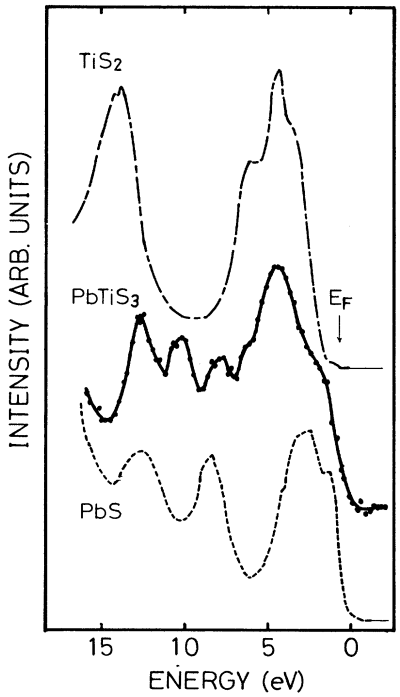


FIG. 4. Valence-band XPS spectrum of $PbTiS_3$, which is compared with those of $TiS_2$ from Ref. 19 and PbS from Ref. 20. The origin of the horizontal axis is the photoemission thresholds of $PbTiS_3$ and PbS and the Fermi level of $TiS_2$ is located at 0.7 eV below the origin. The peak at 10.3 eV of $PbTiS_3$ is the Mg $K\alpha_{3,4}$ satellites of Pb $5d$ electrons.

TABLE II. Energies in eV of main features of the valence-band XPS spectra of $PbTiS_3$, $TiS_2$, and PbS. The Fermi level or the photoemission threshold of $TiS_2$ is located at 0.7 eV below the origin.

| $PbTiS_3$ | $TiS_2$ | | PbS | Assignment |
|---|---|---|---|---|
| 0 | 0.7[a] | 0.7[b] | 0[c] | Fermi energy or the top of valence bands |
| | | 1.2 | 1.20 | bonding band of Ti—S bonds or Pb—S bonds (mainly S 3*p* character) |
| 2.4 | | | 2.53 | |
| | 3.4 | 2.8 | | |
| 4.4 | 4.4 | 4.6 | | bonding band of Ti—S bonds (mainly S 3*p* character) |
| 6.2 | 6.0 | 6.0 | | |
| 7.8 | | | 8.43 | Pb 6*s* band |
| 10.3 | | | | Mg $K\alpha_{3,4}$ satellite of Pb 5*d* core electrons |
| 12.8 | | | 12.81 | S 3*s* band in PbS |
| | 14.0 | | | S 3*s* band in $TiS_2$ |
| 18.6 | | | 18.52 | Pb $5d_{5/2}$ level |
| 21.2 | | | 21.10 | Pb $5d_{3/2}$ level |

[a]Wertheim, DiSalvo, and Buchanan, Ref. 19.
[b]Shephard and Williams, Ref. 21.
[c]McFeely *et al.*, Ref. 20.

$Fe_{1/3}TiS_2$, the iron intercalation derivative of $TiS_2$. The absorption edge is 2467.4 eV for $TiS_2$, 2467.7 eV for $PbTiS_3$ and $Fe_{1/3}TiS_2$, and 2468.3 eV for PbS. Here it is worthwhile to recall that two peaks at initial absorption for $TiS_2$ are ascribed to Ti 3*d* $t_{2g}$ and $e_g$ bands with S 3*p* character and a higher-energy broad peak around 10 eV above the edge is ascribed to Ti 4*s* and 4*p* bands and that intercalation of Fe atoms gives rise to charge transfer from inserted atoms to host layers. Since the $t_{2g}$ band is filled by transferred electrons upon intercalation, the Ti 3*d* $t_{2g}$ peak declines and the absorption edge shifts to higher energy. These facts have been discussed in other papers[27,28] in detail. The rigid band model seems to be valid to the first approximation for interpretation of variations in optical spectra and physical properties. In Fig. 5 we find the same decline of the $t_{2g}$ peak and the higher-energy shift of the absorption edge as observed for the iron intercalation derivative. This change arises evidently from charge transfer from PbS to $TiS_2$ layers. It is also found that for $PbTiS_3$ initial absorption enlarges with a more gentle downslope as compared with $TiS_2$. This is caused by the additional contribution of unoccupied energy states within a PbS layer. The S *K* spectrum in PbS shows a large peak arising from the antibonding levels of Pb—S bonds near the edge. Thus we may conclude that the conduction band is also represented by simple superposition of unoccupied energy bands of each layer and its bottom consists of the Ti 3*d* $t_{2g}$ levels within a $TiS_2$ layer which may overlap the antibonding levels of the PbS bonds.

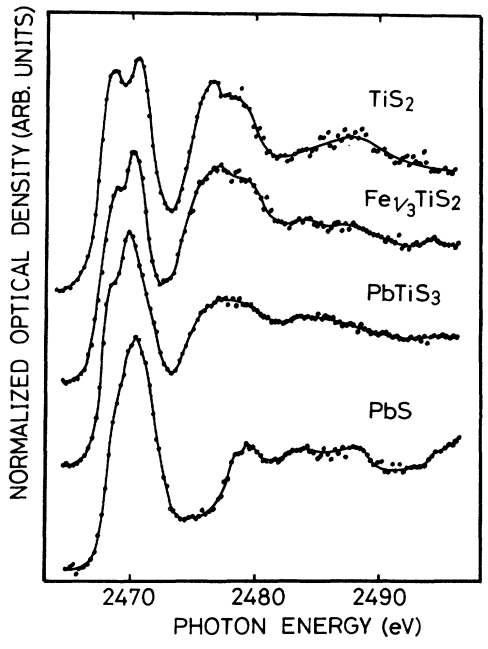


FIG. 5. S *K* XAS spectra of $PbTiS_3$, $TiS_2$, PbS, and $Fe_{1/3}TiS_2$. They are normalized by a maximum absorption intensity.

Figure 6 shows the Ti $M_{2,3}$ and S $L_{2,3}$ inner-shell-electron-energy-loss-spectroscopy (ISEELS) spectra at low incident energy. Since in REELS optically forbidden transitions become possible at low incident energy due to breakdown of dipole selection rules and exchange interaction between incident and excited electrons, its spectrum generally varies with $E_0$.[29–31] The previous ISEELS study of $TiS_2$ (Ref. 14) confirms that the Ti $M_{2,3}$ and S $L_{2,3}$ spectra change with $E_0$ and the Ti 3*d* $t_{2g}$ peak enlarges relative to the $e_g$ peak with decreasing $E_0$. The same variation is observed for $PbTiS_3$. As $E_0$ decreases, the intensity ratio of the $t_{2g}$ peak to the $e_g$ peak is reversed and the former is larger than the latter at $E_0 = 165$ eV. In the Ti $M_{2,3}$ spectrum we see a larger $t_{2g}$-$e_g$ splitting relative to the ones in the S $L_{2,3}$ ISEELS and the S *K*

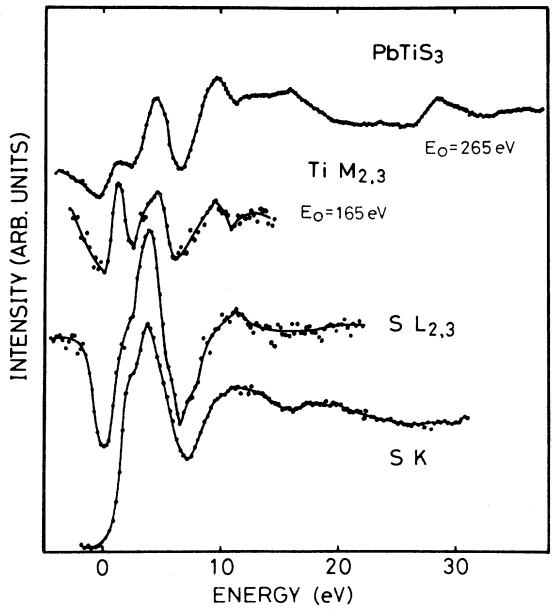


FIG. 6. Ti $M_{2,3}$ and S $L_{2,3}$ ISEELS spectra of $PbTiS_3$, which are compared with the S $K$ XAS spectrum. The ISEELS spectra have been measured in reflection geometry in the second-derivative mode, using a lock-in amplifier. The incident energy $E_0$ is 500 eV for the S $L_{2,3}$ ISEELS spectrum. The loss structures around 30 eV above the Ti $M_{2,3}$ threshold are caused by excitations of Ti 3$s$ core electrons.

XAS spectra, while the latter two spectra exhibit the same crystal-field splitting. Such a trend has already been observed in $TiS_2$ and reduced to the local nature of the spectra (the S $K$ XAS and the S $L_{2,3}$ ISEELS spectra represent unoccupied energy states near excited S atoms while the Ti $M_{2,3}$ ISEELS spectrum represents unoccupied states near excited Ti atoms) and the crystal-field effect which may play an important role for a local electronic structure. For comparison, the S $K$ XAS spectrum is drawn again in Fig. 6. Finally, it is noted that since the mean free path of electrons, in this case, is so small that they reveal selectively only the electronic structure of a top $TiS_2$ layer of a sample, the overall features resemble those of $TiS_2$.

Figure 7 shows the valence-electron-energy-loss-spectroscopy (VEELS) spectra of $PbTiS_3$ and $TiS_2$ at $E_0=100$ eV when the mean free path of electrons has a minimum. In this case the top surface of a measured $PbTiS_3$ sample is constructed of a $TiS_2$ layer and the spectrum picks up the electronic structure. Figure 7 shows a good agreement between the spectra, suggesting that interlayer interaction between $TiS_2$ and PbS layers is very small. Here it is worth noting that energy losses in the range up to 10 eV arise from interband transitions from valence to conduction bands and the peak energies approximately give the root-mean-square values of the transition energies, weighted by their respective oscillator strength, that is,

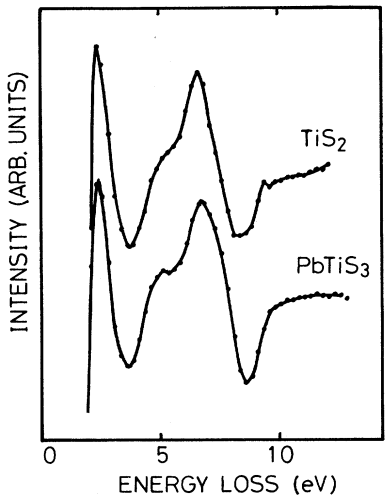


FIG. 7. REELS spectra of $PbTiS_3$ and $TiS_2$, which have been measured at $E_0=100$ eV when the mean free path of electrons is minimum, about 3–5 Å. Since in our measuring system the surface of the former compound is also constructed of a $TiS_2$ layer and a sampling depth is smaller by 2.4 times than the mean free path, detected electrons are reflected dominantly from a top $TiS_2$ layer in both cases.

$$\left[\frac{1}{N}\sum_{v\to c} f_{vc}E_{vc}^2\right]^{1/2},$$

where $N$ is the number of electrons participating in transitions and $f_{vc}$ is the oscillator strength. For $TiS_2$ two peaks at 2.5 and 6.8 eV and a shoulder at 5.0 eV involve the transitions to unoccupied Ti 3$d$ $t_{2g}$ and $e_g$ states. Since the metal $s$ and $p$ bands exist around 10 eV above

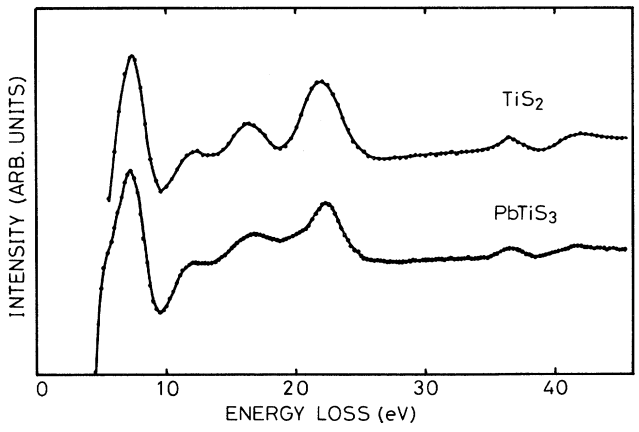


FIG. 8. REELS spectra of $PbTiS_3$ and $TiS_2$ at $E_0=400$ eV. The surface of $PbTiS_3$ is constructed of a $TiS_2$ layer. A bulk-plasmon peak appears at 22.3 and 21.9 eV for $PbTiS_3$ and $TiS_2$, respectively. Peaks around 36 eV are caused by excitation of Ti 3$p$ core electrons.

the Fermi level, the related peaks appear at higher energies as well as surface- and bulk-plasmon peaks. A detailed comparison suggests that for $PbTiS_3$ energy losses in each subband occur at lower energy by charge transfer from PbS layers to $TiS_2$ layers which causes the shift of the Fermi level of $TiS_2$ layers. Another charge-transfer effect is observed in Fig. 8 in which the plasmon peaks are compared. Charge transfer to $TiS_2$ layers gives rise to the shift of a plasmon peak to higher energy by the increase in the number of electrons participating in plasma oscillations. The peak energy for $PbTiS_2$ is 22.3 eV, which is larger by 0.4 eV than that for $TiS_2$. This change corresponds to the increase by 0.7 electrons per unit cell.

### B. $SnNbS_3$

$SnNbS_3$ is constructed by alternately stacking a metallic $NbS_2$ layer and a semiconducting SnS layer which is identical to a double layer in $\beta$-SnS, the high-temperature phase of the compound. If interlayer interaction is very small, bonding within a SnS layer would be similar to that of $\beta$-SnS. Since unfortunately no XPS data have been available for $\beta$-SnS, the binding energies of core electrons of $SnNbS_3$ are compared with those of the $\alpha$ phase[15] in Table III. $\alpha$-SnS crystallizes in the GeS structure which is closely related to the TlI structure of the $\beta$ phase with a distorted NaCl atomic arrangement, although within each layer there is a change in the number of a coordination from 3+2 to 4+1 while going from $\alpha$- to $\beta$-SnS. We find that there is a good agreement between the binding energies of Sn $3d_{5/2}$ and $3d_{3/2}$ electrons of $SnNbS_3$ and $\alpha$-SnS, although a large disagreement exists for S $2s$ and $2p$ electrons. The disagreement is partly caused by the systematic error as described in Sec. III A and partly caused by the chemical shift arising from different chemical circumstances. For $SnNbS_3$ the S $2p$ XPS spectrum reveals only a broad peak, but not an obvious spin-orbit splitting unlike $PbTiS_3$. It may be caused by the overlap of two different S $2p$ XPS spectra which arise from SnS and $NbS_2$ layers. As far as the present author knows, there are still no experimental binding-energy data for $NbS_2$. Sonntag and Brown[25] have measured the Nb $M_4$ and $M_5$ absorption thresholds for $NbSe_2$, but they have mistaken the assignment of the $M_4$ threshold and given a very large $M_{4,5}$ spin-orbit splitting. Then the data have not been referred to in Table III. The present core XPS results suggest that S atoms within a SnS layer are in a different chemical circumstance from those within a $NbS_2$ layer. However, they give no evidence for charge transfer and interlayer interaction.

Figure 9 shows the valence-band XPS spectrum of $SnNbS_3$, which is compared with those of $NbSe_2$ (Ref. 19) and $\alpha$-SnS,[32] because no valence-band XPS spectra of $NbS_2$ and $\beta$-SnS have been available. Many band calculations and experimental results[24–26] suggest that the energy band structure of $NbS_2$ is quite similar to that of $NbSe_2$ and the top of the valence band consists of Nb $d_{z^2}$ levels which are half filled by electrons. The densities of states of $\alpha$-SnS and $\beta$-SnS have been examined by Tremel and Hoffman[33] in the line of the structural and electronic study of the phase transition from the GeS type to the TlI type. According to the result, some states are pushed down and some are stabilized by the transition, but the overall effect is small. In the XPS spectrum of $SnNbS_3$ the S $3s$ bands in the range of 10 to 15 eV are affected by the Mg $K\alpha_{3,4}$ satellites of Sn $4d$ core electrons (binding energies of 24.8 and 25.7 eV). The main valence-band region, on the other hand, represents the energy band structures. The main features are easily assigned, based on the valence-band structures of $NbSe_2$ and $\alpha$-SnS. The results are summarized in Table IV. As can be seen from Fig. 9 charge transfer from a SnS to a $NbS_2$ layer causes both the growth of a shoulder corresponding to the Nb $d_{z^2}$ band and the shift of the Fermi level to higher energy by 0.8 eV, although the value may be overestimated by bad resolution of our instrument. A shoulder at 7.5 eV corresponds to the Sn $5s$ band. Its location is different by

TABLE III. Binding energies in eV of core electrons of $SnNbS_3$ and $\alpha$-SnS. Energies are referred to the Fermi level of a spectrometer.

| Core electron | $SnNbS_3$ | $\alpha$-SnS[a] |
|---|---|---|
| S $2p$ | 160.4 | 161.1 |
| Nb $3d_{5/2}$ | 202.6 | |
| Nb $3d_{3/2}$ | 205.2 | |
| S $2s$ | 224.5 | 225.5 |
| Nb $3p_{3/2}$ | 361.4 | |
| Nb $3p_{1/2}$ | 377.0 | |
| Sn $3d_{5/2}$ | 485.7 | 485.7 |
| Sn $3d_{3/2}$ | 494.0 | 494.1 |

[a]Shalvoy, Fisher, and Stiles, Ref. 15.

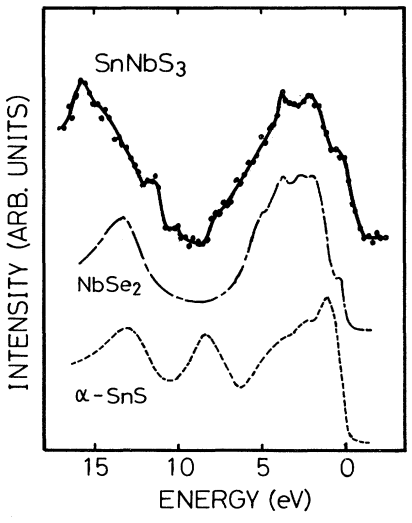


FIG. 9. Valence-band XPS spectrum of $SnNbS_3$, which has been compared with those of $NbSe_2$ from Ref. 19 and PbS from Ref. 32. The structures in the range of 10–15 eV are affected by the Mg $K\alpha_{3,4}$ satellites of Pb $5d$ core electrons.

TABLE IV. Energies in eV of main features of the valence-band photoemission spectra of $SnNbS_3$ $3R$-$NbS_2$, $2H$-$NbSe_2$, and $\alpha$-SnS. The data of $3R$-$NbS_2$ are ultraviolet photoemission data and the others are XPS data.

| $SnNbS_3$ | $3R$-$NbS_2$[a] | $2H$-$NbSe_2$[b] | $\alpha$-SnS | | Assignment |
|---|---|---|---|---|---|
| −0.8 | 0 | 0 | 0[c] | 0[d] | Fermi energy or the top of valence bands |
| 0.5 | 0.6 | 0.5 | | | Nb $4d_{z^2}$ band |
| | | | 1.0 | 1.5 | bonding band of Sn—S bonds (mainly S $3p$ character) or bonding band of Nb—S (Se) bonds (mainly S $3p$ or Se $4p$ character) |
| 2.0 | 2.9 | 2.1 | 2.5 | 2.9 | |
| 3.7 | 3.8 | 3.7 | | | |
| | | | 4.5 | | |
| | 5.5 | 5.0 | | | |
| 7.6 | | | 8.5 | 7.4 | Sn $5s$ band |
| | | 13.3 | 13.3 | | S $3s$ or Se $4s$ band |
| 15.8 | | | | | Mg $K\alpha_{3,4}$ satellite of Sn $4d$ core electrons |

[a]Clark, Ref. 34.
[b]Wertheim, DiSalvo, and Buchanan, Ref. 19.
[c]Kemeny *et al.*, Ref. 32.
[d]Shalvoy, Fisher, and Stiles, Ref. 35.

0.9 eV from the peak position of bulk $\alpha$-SnS measured by Kemeny *et al.*,[32] but is in good agreement with that by Shalvoy, Fisher, and Stiles.[35] Finally, we may conclude that the valence-band structure of each layer is not so largely changed from that of the bulk compound and the overall structures are well represented by simple superposition of the electronic structure of each layer except for charge-transfer effects.

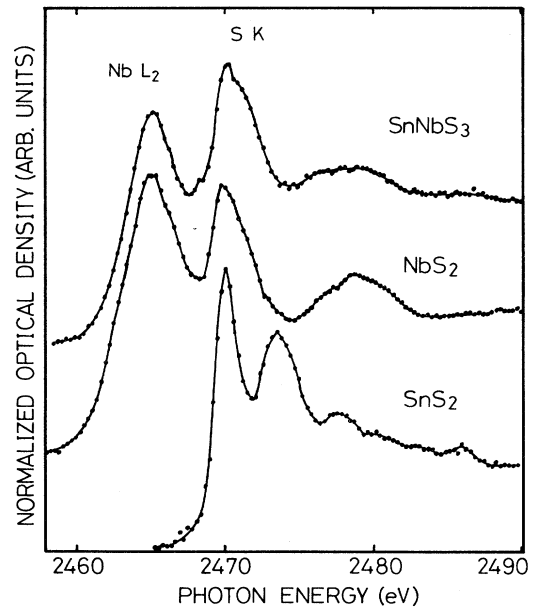


FIG. 10. Nb $L_2$ and S $K$ XAS spectra of $SnNbS_3$, which have been compared with those of $NbS_2$ and the S $K$ spectrum of $SnS_2$.

Unoccupied energy states have been studied by means of the XAS method. The result is shown in Fig. 10 in which the Nb $L_2$ and S $K$ XAS spectra are compared with those of $NbS_2$ and the S $K$ spectrum of $SnS_2$. The near-edge structures of S $K$ absorption are disturbed, because its absorption overlaps Nb $L_2$ absorption. In the previous study of $NbS_2$ (Ref. 27) the present author has picked up the S $K$ spectrum by subtracting the Nb $L_3$ spectrum, assuming that the $L_3$ spectrum exhibits the same structures as the $L_2$ spectrum. The resulting S $K$ spectrum as well as the Nb $L_2$ spectrum has a shoulder near the edge, which has been assigned to unoccupied energy states in the incompletely filled Nb $d_{z^2}$ band. This shoulder declines upon intercalation of Sn and Cu atoms due to charge transfer from intercalates to host layers, because transferred electrons occupy the $d_{z^2}$ band.[36] For $SnNbS_3$ the same phenomenon is observed, that is, we observe no shoulders near the edge and the absorption edge shifts to higher energy as compared with $NbS_2$. Then we may conclude that charge transfer occurs from SnS to $NbS_2$ layers, in agreement with the valence-band XPS results. Consequently, the compound may be regarded as the intercalation derivative of $NbS_2$. In this case SnS acts as a donor type of intercalate which forms a double layer within a van der Waals gap. In another point of view, however, it may be regarded as a material having a one-dimensional superlattice with an atomic-scale repeat distance. The electronic structure of each layer is quite similar to that of the bulk compound. The intensity ratio of the S $K$ absorption peak to the Nb $L_2$ peak is larger for

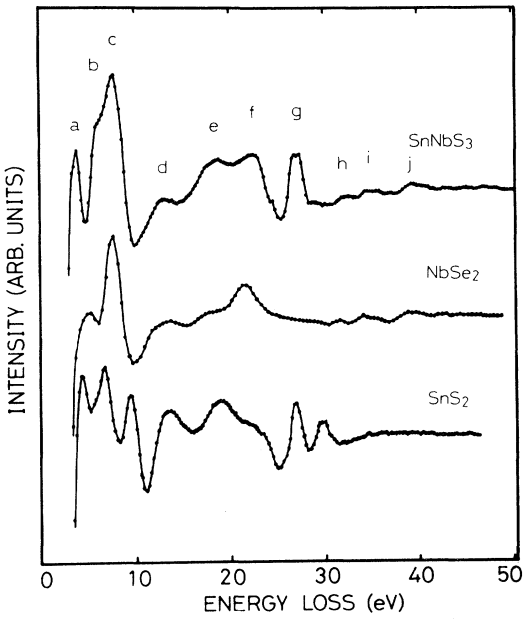


FIG. 11. REELS spectra of $SnNbS_3$, $NbSe_2$, and $SnS_2$. They have been measured at $E_0=200$ eV in the second-derivative mode. The ionization thresholds of Sn 4*d* and Nb 4*d* core electrons are about 25 and 32 eV, respectively.

$SnNbS_3$ than for $NbS_2$. This is a clear evidence for additional contribution for unoccupied energy states of SnS layers.

Here it should be noted that the S *K* spectrum in $SnS_2$ exhibits a large peak around 5 eV above the edge, but the S *K* spectrum in $SnNbS_3$ does not show the peak (see Fig. 10). The same result has been obtained from the energy-loss spectra for excitation of Sn 4*d* core electrons. Figure 11 shows the REELS spectra of $SnNbS_3$, $NbSe_2$, and $SnS_2$, which have been measured at $E_0=200$ eV. Since the measured surface of $SnNbS_3$ is formed by many steps, the REELS spectrum gives information about core-electron transitions, interband transitions, and collective excitations from both SnS and $NbS_2$ layers. The ionization threshold of Sn 4*d* electrons is about 25 eV. Then the fine structures in the range of 25–30 eV may be reduced to excitation of Sn 4*d* electrons. As can be seen from Fig. 11 the REELS spectrum exhibits only a peak in the energy region, but the spectrum of $SnS_2$ reveals the two peaks as observed in the S K XAS spectrum. The difference arises from the different energy band structures of SnS and $SnS_2$. As far as the present author knows, few band calculations and experiments have been carried out for unoccupied energy states of SnS. Then the detailed examination of the conduction band has not been made. For $SnS_2$, on the other hand, there are many band calculations and experimental results.[26,37–39] According to the results, the lower conduction bands consist of two bands with different character; one is derived primarily from Sn 5*s* states and the other is from Sn 5*p* states. The above two peaks correspond to the two energy bands. The REELS spectrum of $SnNbS_3$ exhibits no peak at 9.2 eV unlike the spectrum of $SnS_2$, because the loss peak arises from the transitions to the upper 5*p* conduction band. The REELS results are summarized in Table V. Since energy resolution increases with decreasing $E_0$, most of the energy values have been estimated at $E_0=100$ eV. The incident-energy dependence is shown in Fig. 12 and the assignments have been made by comparison with the loss structures of $NbSe_2$ and $SnS_2$ which have already been determined by Bell and Liang[40] and Ohno.[39] The free plasmon energies of $NbS_2$ and SnS have been calculated, using the relation $E_p=(\hbar^2e^2n/\epsilon_0 m)^{1/2}$, where $n$ is the electron density per unit volume and referring to the lattice constants of Refs. 41 and 42. They are 20.3 and 16.9 eV, respectively. These values are smaller by 1–2 eV than the experimental values, which is caused by the breakdown of the simple free-electron model, the higher-energy shift due to interband transitions at lower energies, and the momentum-transfer effect.[39,43]

TABLE V. Energies in eV of main features of the REELS spectrum of $SnNbS_3$. Notations below are shown in Fig. 11.

| Notation | Energy | Assignment |
|---|---|---|
| *a* | 3.5 | interband transitions in SnS and $NbS_2$ layers |
| *b* | 5.7 | |
| *c* | 8.0 | plasmon of *d*-band electrons in $NbS_2$ layers |
| *d* | 12.9 | interband transitions and surface plasmon in SnS layers |
| *e* | 17.5 | bulk plasmon in SnS layers and interband transitions from S 3*s* levels of $NbS_2$ |
| *f* | 22.5 | bulk plasmon in $NbS_2$ layers |
| *g* | 25.8 | Sn $N_5$ transition |
| | 27.1 | Sn $N_4$ transition |
| *h* | 32.2 | |
| *i* | 35.0 | Nb $N_{2,3}$ transition |
| *j* | 39.2 | |

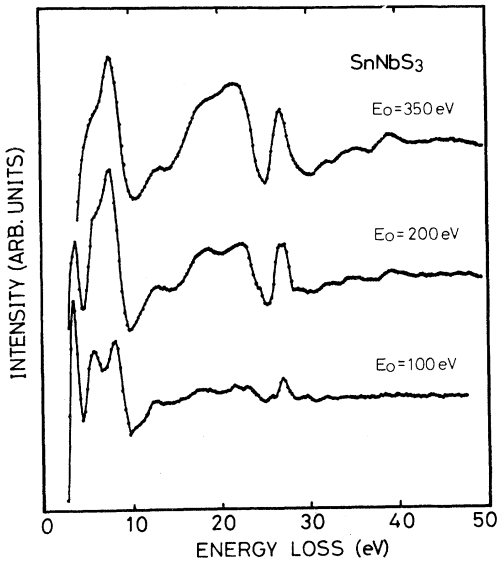


FIG. 12. REELS spectra of $SnNbS_3$ at various incident energies. As $E_0$ decreases, energy resolution increases, but plasmon peaks decline relative to interband-transition peaks and core-electron peaks.

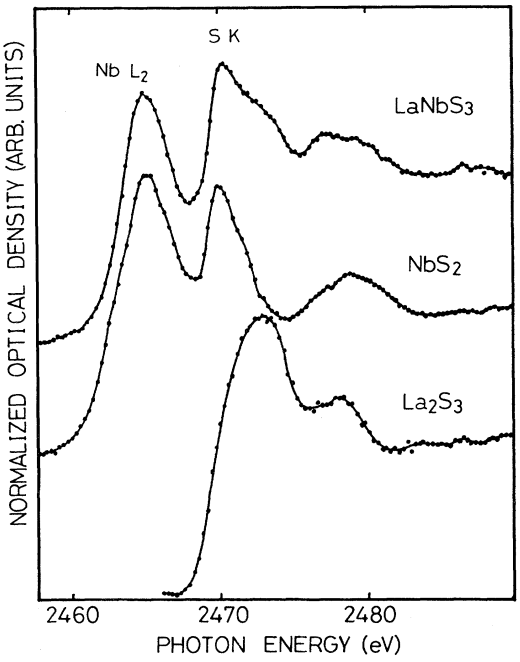


FIG. 13. Nb $L_2$ and S $K$ XAS spectra of $LaNbS_3$, which have been compared with those of $NbS_2$ and S $K$ XAS spectrum of $La_2S_3$.

## IV. CONCLUSIONS

The following conclusions are derived from the present XPS, XAS, and REELS studies.

(1) The compounds $PbTiS_3$ and $SnNbS_3$ are constructed of alternately stacked layers with different electronical and optical properties such as observed in the bulk compounds.

(2) The overall features of the valence and conduction bands are given by the simple superposition of the energy bands of each layer except for charge-transfer effects.

(3) Charge transfer occurs from PbS or SnS layers to the slabs of a transition-metal disulfide by different chemical potentials. The effects on the XPS, XAS, and REELS spectra are quite similar to those of the intercalation compounds of layered transition-metal disulfides. The main effects are related to the shift of the Fermi level and the increase in the number of electrons per unit cell.

(4) Interlayer interaction is so small that we may consider that each layer has a quasi-two-dimensional electronic structure.

(5) The compounds may be regarded as intercalation derivatives of layered transition-metal disulfides. In this case inserted PbS or SnS molecules form a double layer with the TlI structure and have similar electronic band structures to the bulk compound. In another point of view, we may regard them as the compounds having a one-dimensional superlattice with an atomic-scale repeat distance.

## APPENDIX

In relation to the discussion on the XAS spectra of $SnNbS_3$, here we describe the Nb $L_2$ and S $K$ XAS spectra of $LaNbS_3$ which has the same crystal structure. Its lattice is constructed of alternately stacked LaS and $NbS_2$ layers. Figure 13 shows the Nb $L_2$ and S $K$ XAS spectra, which are compared with those of $NbS_2$ and the S $K$ XAS spectrum of $La_2S_3$ instead of LaS, because unfortunately no samples of LaS have been available. It is found that the absorption structures of $LaNbS_3$ are well represented by the simple superposition of those of each layer excluding the charge-transfer effects as described in Sec. III. A shoulder at 2473 eV is derived from the unoccupied energy states of LaS layers while a peak at 2469 eV is derived mainly from the unoccupied Nb $d$ states of $NbS_2$ layers. The results obtained from the spectra support the conclusions in Secs. III and IV.

[1]W. Sterzel, Naturwissenschaften **53**, 199 (1966).
[2]W. Sterzel and J. Horn, Z. Anorg. Allg. Chem. **376**, 254 (1970).
[3]P. C. Donohue, J. Solid State Chem. **12**, 80 (1975).
[4]T. Murugesan, S. Ramesh, J. Gopalakrishnan, and C. N. R. Rao, J. Solid State Chem. **38**, 165 (1981).
[5]L. Schmidt, Phys. Lett. **31A**, 551 (1970).
[6]L. Schmidt, S. L. McCarthy, and J. P. Maita, Solid State Commun. **8**, 1513 (1970).

[7]M. H. Haaren, Phys. Lett. **40A**, 353 (1972).
[8]G. A. Wiegers, A. Meetsma, R. J. Haange, and J. L. Boer, Mater. Res. Bull. **23**, 1551 (1988); Solid State Ionics **32/33**, 183 (1989).
[9]G. A. Wiegers, A. Meetsma, S. Smaalen, R. J. Haange, J. Wulff, T. Zeinstra, J. L. Boer, S. Kuypers, G. Tendeloo, J. Landuyt, S. Amelinckx, A. Meerschaut, P. Rabu, and J. Rouxel, Solid State Commun. **70**, 409 (1989).
[10]A. Meetsma, G. A. Wiegers, R. J. Haange, and J. L. Boer, Acta Crystallogr. A **45**, 285 (1989).
[11]A. Meerschaut, P. Rabu, and J. Rouxel, C. R. Acad. Sci. Paris **307**, 1513 (1988).
[12]L. Guemas, P. Rabu, A. Meerschaut, and J. Rouxel, Mater. Res. Bull. **23**, 1061 (1988).
[13]Y. Ohno, Bull. Fac. Gen. Edu. Utsunomiya Univ. Sec. 2 **19**, 5 (1986).
[14]Y. Ohno, Phys. Rev. B **36**, 7500 (1987).
[15]R. B. Shalvoy, G. B. Fisher, and P. J. Stiles, Phys. Rev. B **15**, 1680 (1977).
[16]K. Endo, H. Ihara, K. Watanabe, and S. Gonda, J. Solid State Chem. **44**, 268 (1982).
[17]D. W. Fischer, Phys. Rev. B **8**, 3576 (1973).
[18]B. Sonntag and F. C. Brown, Phys. Rev. B **10**, 2300 (1974).
[19]G. K. Wertheim, F. J. DiSalvo, and D. N. E. Buchanan, Solid State Commun. **13**, 1225 (1973).
[20]F. R. McFeely, S. Kowalczyk, L. Ley, R. A. Pollak, and D. A. Shirley, Phys. Rev. B **7**, 5228 (1973).
[21]F. R. Shepherd and P. M. Williams, J. Phys. C **7**, 4416 (1974).
[22]S. E. Kohn, P. Y. Yu, Y. Petroff, Y. R. Shen, Y. Tsang, and M. L. Cohen, Phys. Rev. B **8**, 1477 (1973).
[23]T. Grandke, L. Ley, and M. Cardona, Phys. Rev. B **18**, 3847 (1978).
[24]*Electrons and Phonons in Layered Crystal Structures,* edited by T. J. Wieting and M. Schluter (Reidel, Boston, 1979).
[25]*Optical and Electrical Properties,* edited by P. A. Lee (Reidel, Boston, 1976).
[26]*Electronic Structures and Electronic Transitions in Layered Materials,* edited by V. Grasso (Reidel, Boston, 1986).
[27]Y. Ohno, K. Hirama, S. Nakai, C. Sugiura, and S. Okada, Phys. Rev. B **27**, 3811 (1983).
[28]Y. Ohno, K. Hirama, S. Nakai, C. Sugiura, and S. Okada, Synth. Metals **6**, 149 (1983).
[29]J. A. D. Matthew, G. Strasser, and F. P. Netzer, Phys. Rev. B **27**, 5839 (1983).
[30]G. Strasser, G. Rosina, J. A. D. Matthew, and F. P. Netzer, J. Phys. F **15**, 739 (1985).
[31]Y. Ohno, J. Phys. Soc. Jpn. **56**, 3695 (1987).
[32]P. C. Kemeny, J. Azoulay, M. Cardona, and L. Ley, Nuovo Cimento B **39**, 709 (1977).
[33]W. Tremel and R. Hoffman, Inorg. Chem. **26**, 118 (1987).
[34]W. B. Clark, J. Phys. C **9**, L693 (1976).
[35]R. B. Shalvoy, G. B. Fisher, and P. J. Stiles, Phys. Rev. B **15**, 2021 (1977).
[36]Y. Ohno, K. Kaneda, and K. Hirama, Phys. Rev. B **30**, 4648 (1984).
[37]G. Margaritondo, J. E. Rowe, M. Schlüter, and H. Kasper, Solid State Commun. **22**, 753 (1977).
[38]Y. Gao, B. Smandek, T. J. Wagener, J. H. Weaver, F. Lévy, and G. Margaritondo, Phys. Rev. B **35**, 9357 (1987); **37**, 4196 (1988).
[39]Y. Ohno, J. Phys. Soc. Jpn. **59**, 3740 (1990).
[40]M. G. Bell and W. Y. Liang, Adv. Phys. **25**, 53 (1976).
[41]R. M. A. Lieth and J. C. J. M. Terhell, in *Preparation and Crystal Growth of Materials with Layered Structures,* edited by R. M. A. Lieth (Reidel, Boston, 1977).
[42]H. G. Schnering and H. Wiedemeier, Z. Kristallogr. **156**, 143 (1981).
[43]H. Raether, in *Excitations of Plasmons and Interband Transitions by Electrons,* edited by G. Hohler (Springer-Verlag, New York, 1980).